Short Communication

Nano Iron Oxides/Sisal Fiber Carbons Composites as Anode Materials for Lithium-ion Batteries

Rui Du [1,2] *, Zhangfa Tong* [1] *, Chun Wei* [1,2] *, Aimiao Qin* [2,3*] *, Kaiyou Zhang* [2] *, Lei Liao* [2]

[1] School of Chemistry and Chemical Engineering, Guangxi University, Nanning 530001, PR China
[2] Guangxi Ministry-Province Jointly-Constructed Cultivation Base for State Key Laboratory of Processing for Non-ferrous Metal and Featured Materials, Guilin University of Technology, Guilin 541004, PR China.
[3] Guangxi Experiment Center of Information Science, Guilin 541004, Guangxi, PR China
[*]E-mail: 317881264@qq.com

A new microporous carbon was obtained by pyrolysis of sisal fibers. And nano iron oxides/sisal fiber carbons composites were synthesized by hydrothermal method. The structure of the compositets were characterized by XRD and SEM, and the influence of hydrothermal temperature on the electrochemical performance of the composites was studied by cyclic voltammetry and constant current charge and discharge tests. The results show that the structure of nano iron oxides varied with hydrothermal temperatures. As anode materials for lithium-ion batteries, the composites showed a wonderful synergistic effect on the electrochemical performance, and the composites prepared at 120 °C consisted of α-FeOOH and α-Fe$_2$O$_3$ mixture phases and exhibited the highest reversible specific capacity and the best cycling stability.

1. INTRODUCTION

Graphite is widely used as anode materials for lithium-ion batteries (LIBs), which has not been able to meet people's requirements because of the limitation in capacity [1]. Iron oxides have attracted great interests due to their considerable theoretical capacities, high initial coulombic efficiency and good safety. However, the low electronic conductivity of iron oxides and volume change during charge and discharge processes lead to its bad cycling performance [2, 3].

Biomasses contain a large amount of carbon, and the microporous carbons based on biomasses not only possess higher specific capacity than graphite but also perform very good electrochemical

stability as anode materials for LIBs [4-7]. Nevertheless, these pyrolyzed carbons usually have a great shortcoming of low initial coulombic efficiency. Therefore, the composites of iron oxides and pyrolyzed biomasses carbons are expected to exhibit better electrochemical performance in comparison with the individual iron oxides or microporous carbons as a result of the synergistic effect [8-11].

Sisal is the characteristic biomass resource which is planted widely around the world. Sisal fiber is a major by-product in sisal industry. Sisal fibers have excellent mechanical property which are mainly used as textiles, artware and reinforced material [12-15]. Table 1 shows the chemical composition of sisal fiber. Cellulose is the main constituent of sisal fiber. In the sisal fiber, the content of cellulose is 65.8%, which play a important role in preparing carbons. Fig.1 shows the element types of sisal fiber (Data from Energy Disperse Spectroscopy).

By pyrolysis of sisal fibers, a new microporous sisal fiber carbons (SFCs) were obtained, and then the composites of iron oxides and the SFCs were prepared by simple hydrothermal method. As anode materials for LIBs, the iron oxide/SFCs composites exhibited high specific capacity and excellent cycle stability.

Table 1. The chemical composition of sisal fiber

Composition	Cellulose	Hemi-cellulose	Lignin	Pectin	Water	Other materials
Content （%）	65.8	12.0	9.9	0.8	10.0	1.5
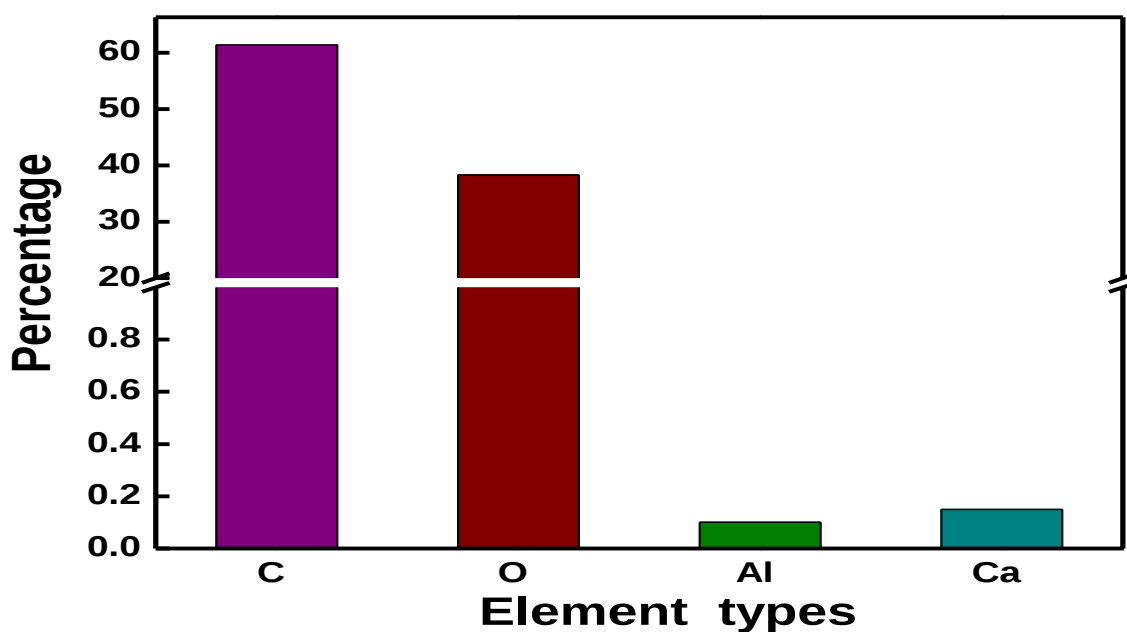
Figure 1. Element types of sisal fiber

2. EXPERIMENTAL

Sisal fibers were supplied by Guangxi sisal group Co. LTD. Sisal fibers were thoroughly washed with distilled water for several times. The washed sisal fibers were dried at 80°C in an oven for 8h and then pyrolyzed at 900°C under the protection of nitrogen for 1h with a heating rate of 3°C /min. After cooling to room temperature naturally, the black carbonized products (sisal fiber carbons, SFCs) were grounded in a planetary ball mill for further use.

The iron oxides/SFCs composites were prepared by hydrothermal method, 0.75g grounded SFCs were dispersed in 80ml mixed solution containing 0.875g ferric chloride ($FeCl_3 \cdot 6H_2O$) and 0.3g urea ($CO(NH_2)_2$) with deionized water as solvent. The mixture was stirred at room temperature for 2h and then transferred into an autoclave lined with PTFE of 80ml in volume. The autoclave was heated at specific temperatures (100°C, 120°C and 140°C) for 14 h. After cooling, the product was filtered and washed repeatedly with deionized water until pH=7. The final composites were obtained by drying at 80°C for 12h in a vacuum oven. The as-prepared composites at different hydrothermal temperatures were named as C-100, C-120 and C-140, respectively.

Powder X-ray diffraction was performed on a PANalytical X'Pert PRO diffractometer with nickel-filtered Cu K α radiation. The data were recorded between scattering angles (2θ) of 10° and 70° in steps of 0.05°. The morphology of the samples was examined by an Oxford S-4800 scanning electron microscope.

Electrochemical property were tested using coin cells (CR2025, half cell) with Li foil as counter electrode. Carbon electrodes electrochemical studies were prepared by blade-coating a slurry containing 80 wt.% of the composites, 10 wt.% of polyvinylidene fluoride (PVDF) and 10 wt.% of acetylene black dispersed in N-methyl-2-pyrrolidinone (NMP) solvent on a copper foil and dried in a vacuum oven at 110°C for 12 h. The cells were assembled in an argon-filled glove box (VACMO40-1). The electrolyte was 1M $LiPF_6$ which was prepared by dissolving $LiPF_6$ in a mixture of ethylene carbonate, dimethyl carbonate and diethyl carbonate with a volume ratio of 1:1:1. And a Celgard 2400 microporous polypropylene film was used as separator. Galvanostatic charge-discharge profiles were recorded between 0.01 and 3.00V at a rate of 0.1 C on a Neware BTS battery test system. In addition, the pure SFCs and commercially available α-Fe_2O_3 were also studied by the same method as a contrast experiment.

3. RESULTS AND DISCUSSION

Fig. 1 shows XRD patterns of iron oxides/SFCs composites prepared under different temperatures. It can be seen that the products exhibit quite different phases as hydrothermal temperature varied. For C-100, the diffraction peaks match well with β-FeOOH (tetragonal, JCPDS Card No. 75-1594). For C-120, the characteristic diffraction peaks of both α-FeOOH (orthorhombic, JCPDS Card No.29-0713) and α-Fe2O3 (rhombohedral, JCPDS Card No. 87-1165) can be found in the pattern. And for C-140, the diffraction peaks can be assigned to the pure α-Fe_2O_3 phase. In the three curves, the narrow sharp peaks indicate the good crystallization of iron oxides. Meanwhile, the

diffraction peaks of graphitized carbon are not detected, which suggests that SFCs in the composites are amorphous structure.

According to the XRD analysis, we can speculate that the phase conversion process of the iron oxides may be as follows: at low temperature of 100°C, β-FeOOH was formed because of the precipitation reaction of $FeCl_3$ and $CO(NH_2)_2$, as the temperature increasing, β-FeOOH converted into α-FeOOH gradually and α-FeOOH further dehydrated into α-Fe$_2$O$_3$.
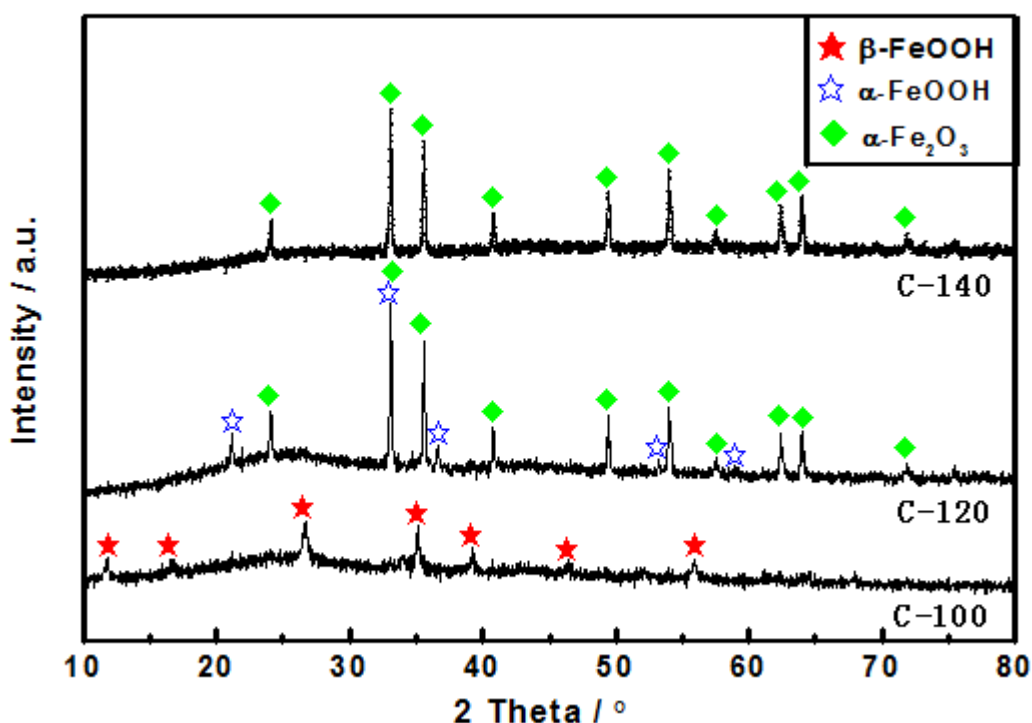
Figure 1. XRD patterns of the three iron oxides/SFCs composites

Fig. 2 shows SEM images of the individual SFCs(without mill) and the iron oxide/SFCs composites. It can be seen that SFCs(without mill) presents a typical honeycomb structure with a large number of micron scale macropores on the cross section. The results show that there also exists a large number of micropores in iron oxide/SFCs composites (such as shown in Fig. 2(c)); and the average pore size based on the Horvath–Kawazoe (HK) model is 2.0 nm. These micropores have lots of locations for lithium storage [16]. The morphology of β-FeOOH shown in Fig. 2(b) displays a typical rod-like particle with size of 100nm in length. The rods observed in the Fig. 2(c) become shorter and rounder, which may be in accordance with the transition state in the process of crystal transformation from α-FeOOH to α-Fe$_2$O$_3$. And the α-Fe$_2$O$_3$ polyhedra with dominant hexahedra nanocrystals can be identified from the Fig. 2(d). These nanocrystals with size of about 100-300 nm are highly aggregated due to the high surface energy, which may affect their electrochemical performances [17].
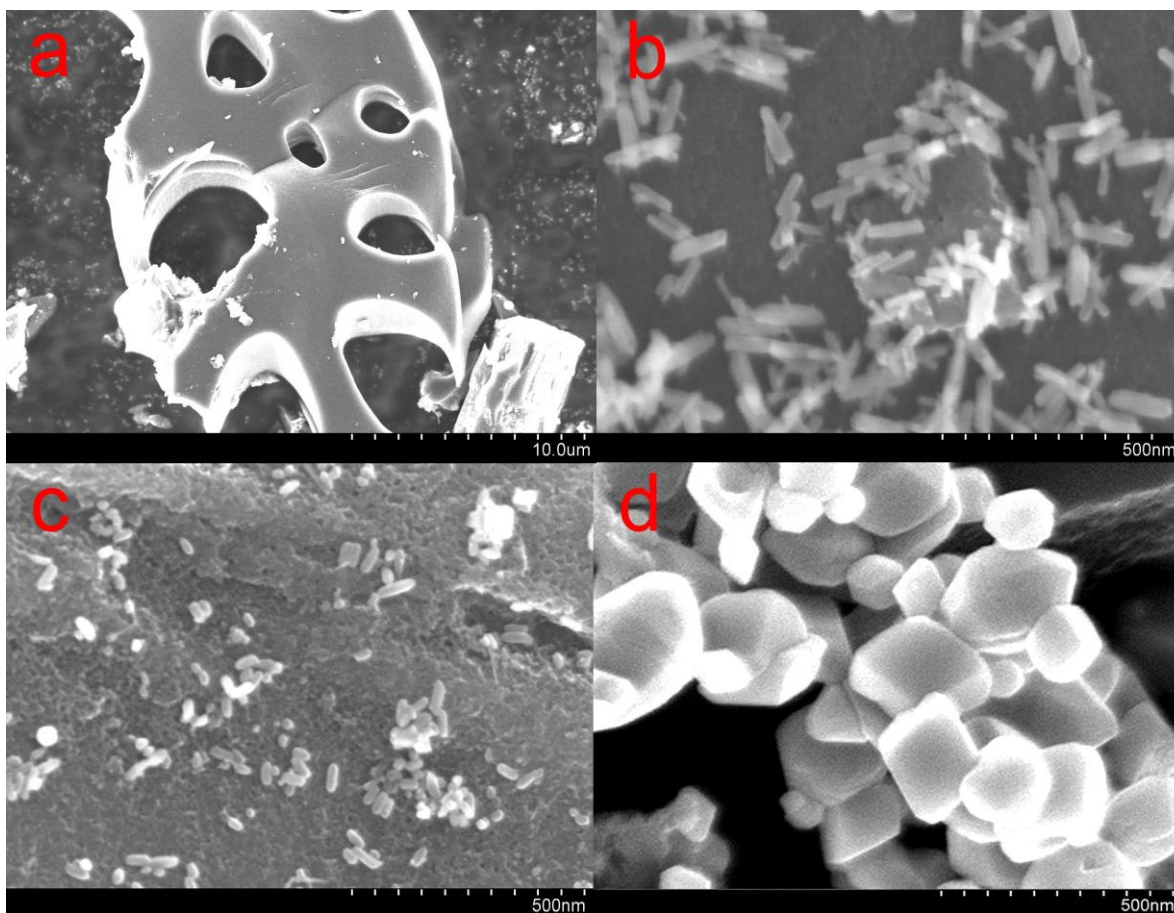
Figure 2. SEM images of SFCs (a), C-100 (b), C-120 (c) and C-140 (d)

The cycling performance curves of the iron oxide/SFCs composites, pure α-Fe$_2$O$_3$ and SFCs tested in the voltage range of 0.01–3.00 V vs. Li/Li+ at a current density of 50 mA/g are shown in Fig. 3(a). It can be seen that the pure α-Fe$_2$O$_3$ possesses the highest specific capacity of 1137 mAh/g for the first cycle, exceeding its theoretical specific capacity of 1007 mAh/g. The result was caused by the low-voltage decomposition of the electrolyte and subsequent formation of an organic layer deposited on the surface of the particles [18]. However, a serious fade appears with the increase of cycle number, which may arise from the collapse of the structure of Fe$_2$O$_3$ caused by the volume change during lithium intercalation and deintercalation processes [3]. It should be noted that the composites appear obviously higher specific capacity than individual SFCs and better cycling stability than individual α-Fe$_2$O$_3$. Through comprehensive comparison, C-120 exhibits the highest reversible specific capacity and the best cycling stability.

In view of the better electrochemical performance of C-120 composite, its discharge/charge curves are analyzed for the further investigation. As shown in Fig. 3(b), the lithium insertion specific capacity of 754 mAh/g is obtained from the first cycle, and the corresponding reversible specific capacity is 440 mAh/g. The initial coulombic efficiency of C-120 composite of 58% is higher than the individual SFCs of 41% but lower than the pure α-Fe$_2$O$_3$ of 70%. The irreversible specific capacity in the first cycle can be mainly attributed to the formation of solid electrolyte interphase (SEI) layer

which is caused by the decomposition of electrolyte on the surface of the electrode [19]. In the subsequent cycles, C-120 exhibits a coulombic efficiency higher than 90% and reaches to nearly 100% after the tenth cycle. In the first discharge curve, an obvious plateau at 0.8 V can be found, suggesting the reduction reaction of Fe^{3+} reducing to Fe^0 and the formation of Li_2O in the electrode material [4]. The reaction equations may be described as follows:

$$\alpha\text{-FeOOH} + 3Li^+ + 3e \rightarrow Fe + LiOH + Li_2O \qquad (1)$$

$$\alpha\text{-Fe}_2O_3 + 6Li^+ + 6e \rightarrow 2Fe + 3Li_2O \qquad (2)$$
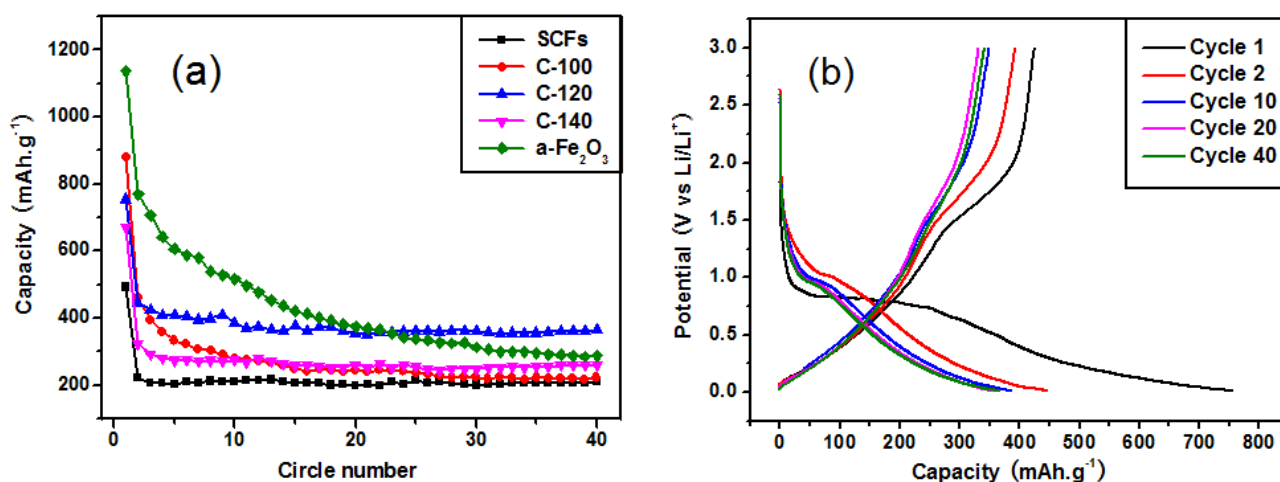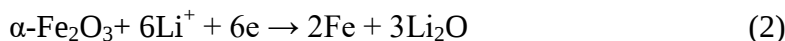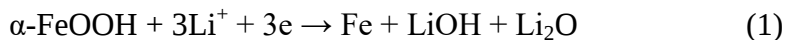
Figure 3. Cycling performance curves of the electrodes based on SFCs, iron oxide/SFCs composites and pure $\alpha\text{-Fe}_2O_3$ (a), and the discharge/charge curves of the electrodes based on C-120 (b)

Besides, a potential plateau at 0.8-0.9 V is an indication of lithium insertion into the porous structure of the iron oxide/SFCs composite without changing the Fe_2O_3 structure. The discharge curves after the second cycle are quite different from the first one, illustrating that the irreversible lithium insertion reaction occurs in the first cycle [20]. In the all charge curves, the long gradient plateau appears in the range of 1.5-2.2 V corresponding to the oxidation reaction of Fe^0 to Fe^{3+}. What's more, the C-120 composite maintains the highest discharge specific capacity of 359 mAh/g after forty cycles among all the tested samples, and the corresponding specific capacity retention is 82%. On the whole, the existence of SFCs will contribute to improve the cycling performance of the composites, but at the cost of the reduction of initial coulombic efficiency [21].

4. CONCLUSIONS

The nano iron oxides/SFCs composites have been prepared by hydrothermal method. The morphology and phase structure of iron oxides in the composites are dependent on the hydrothermal temperature. Nano iron oxides/SFCs composites exhibited better electrochemical performance than that of individual SFCs and Fe_2O_3 as a result of synergistic effect. Especially for C-120, the high

specific capacity and excellent cycling stability may be closely associated with the uniform size, shape, and surface area of iron oxides.

Reference

1. J. M. Tarascon, M. armand, *Nature,* 414 (2011) 359.
2. M. Li, Y. Wang, C. Liu, H. Gao, W. Dong, *Electrochimica Acta*, 67 (2012) 187.
3. Y. Li, C. Zhu, T. Lu, Z. Guo, D. Zhang, J. Ma, S. Zhu. *Carbon*, 52 (2013) 565.
4. X. Sun, X. Wang, N. Feng, L. Qiao, X. Li, D. He, *Journal of Analytical and Applied Pyrolysis*, 100 (2013) 181.
5. S. Bhardwaj, M. Sharon, T. Ishihara, S. Jayabhay, *Carbon Letters*, 8 (2007) 285.
6. T. Zhou, H. Wang, S. Ji, H. Feng, R. Wang, *Fuel Cells*, 14 (2014) 296.
7. H. Yang, H. Wang, S. Ji, Y. Ma, V. Linkov, R. Wang, *Journal of Solid State Electrochemistry*, 18 (2014) 1503.
8. Y. Huang, Z. Dong, D. Jia, Z. Guo, W. Cho, *Solid State Ionics*, 201 (2011) 54.
9. C. Wu, X, Li, W. Li, B. Li, Y. Wang, Y. Wang, M. Xu, L. Xing, *Journal of Power Sources*, 251 (2014) 85.
10. H. Liu, W. David, G. Wang, *Journal of Alloys and Compounds*, 487 (2009) L24.
11. P. Yiseul, O. Misol, S. P. Jung, *Carbon*, 94 (2015) 9.
12. Y. Li, Y. W. Mai, L. Ye, *Composites Science and Technology*, 60 (2000) 2037.
13. S. Mishra, A. k. Mohanty, L. T. Drzal, M. Misra, G. Hinrichsen, *Macromolecular Materials and Engineering*, 11 (2004) 289.
14. I. D. Ibrahim, T. Jamiru, E. R. Sadiku, W. K. Kupolati, S. C. Agwuncha, G. Ekundayo, *Composite Interfaces*, 23 (2016) 15.
15. M. A. Khan, S. Guru, P. Padmakaran, D. Mishra, M. Mudgal, S. Dhakad, *Composite Interfaces*, 18 (2011) 527.
16. J. Hu, H. Li, X. Huang. *Solid State Ionics*, 176 (2005) 1151.
17. J. Wang, C. Zhong, D. Wexler, N. H. Idris, Z. Wang, L. Chen, H. Liu, *Chemistry-A European Journal*, 17 (2011) 661.
18. D. Larcher, D. Bonnin, R. Cortes, I. Rivals, L. Personnaz, J. M. Tarascon, *Journal of The Electrochemical Society* 150 (2003) A1643.
19. P. G. Bruce, B. Scrosati, J. M. Tarascon, *Angewandte Chemie International Edition*, 47 (2008) 2930.
20. N. Liu, J. Shen, D. Liu, *Electrochimica Acta*, 97 (2013) 271.
21. Y. Sun, J. Zhang, T. Huang, Z. Liu, A. Yu, *International Journal of Electrochemical Science*, 8 (2013) 2918.